

Boundary spin polarization as robust signature of topological phase transition in Majorana nanowires

Marcel Serina, Daniel Loss, and Jelena Klinovaja

Department of Physics, University of Basel, Klingelbergstrasse 82, CH-4056 Basel, Switzerland

(Dated: August 22, 2018)

We show that the boundary charge and spin can be used as alternative signatures of the topological phase transition in topological models such as semiconducting nanowires with strong Rashba spin-orbit interaction in the presence of a magnetic field and in proximity to an s -wave superconductor. We identify signatures of the topological phase transition that do not rely on the presence of Majorana zero-energy modes and, thus, can serve as independent probes of topological properties. The boundary spin component along the magnetic field, obtained by summing contributions from all states below the Fermi level, has a pronounced peak at the topological phase transition point. Generally, such signatures can be observed at boundaries between topological and trivial sections in nanowires and are stable against disorder.

I. INTRODUCTION

Topological models have attracted a lot of attention in recent years. One of the first topological systems proposed about forty years ago is the Su-Schrieffer-Heeger (SSH) model¹, describing properties of one-dimensional dimerized polymers. In this spinless model, a nondegenerate fermionic zero-mode, localized at a domain wall, is associated with a well-defined half-integer boundary charge^{2,3}. The same results were first predicted in a continuum model proposed by Jackiw and Rebbi⁴. The half-integer value of the boundary charge in these models is protected by the chiral symmetry. If this symmetry is broken, the value of the boundary charge can deviate from $e/2$ ^{5,6}. Importantly, however, in the topological regime, there is always a boundary charge (independent of the presence of bound states) at the domain wall as was shown in several extensions of the SSH model⁷⁻⁹. Recently, the concept of the fractional boundary charge in topological SSH models was revisited, aiming at different systems that could be realized in modern experimental settings¹⁰⁻²⁸ and even in higher dimensions²⁹⁻³¹. Motivated by these studies on boundary charges we would like to go a step further and focus in this work on boundary spins. In particular, we want to study the behavior of boundary spins in- and outside the topological phase and demonstrate that the total moment of spins close to the boundary can be used as signature for the topological phase transition.

Currently, Majorana fermions (MFs), proposed as a real-field solution of the Dirac equation and thus being its own antiparticle³², attract the most attention among the known bound states in topological systems. With the rapidly growing interest in topological properties of condensed matter systems³³⁻³⁹, MFs were proposed to be present in various theoretical and experimental setups⁴⁰⁻⁵⁶. The most promising ones among them being chains of magnetic adatoms on superconducting surfaces⁵⁷⁻⁵⁹ and semiconducting nanowires (NWs) with sizeable Rashba spin-orbit interaction (SOI) in the presence of a magnetic field and proximity-induced supercon-

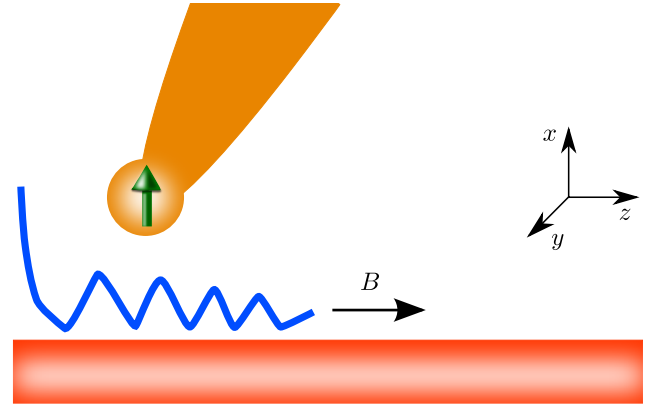


Figure 1. Our setup consists of a semiconducting NW (red bar) with Rashba SOI and with proximity-induced superconductivity due to coupling to a bulk s -wave superconductor (not shown). The SOI vector α points along the y direction. A magnetic field \mathbf{B} applied along the NW axis is used to tune the system in and out of the topological phase. The boundary spin accumulates at the edges of the NW (blue curve) and can be used to identify the topological phase transition point. The magnetic signal can be measured by using $e.g.$ NV centers (green arrow) on a tip (orange).

ductivity⁶⁰⁻⁶⁴. Majorana fermions can be used as building blocks for topological quantum computing^{65,66} and can be combined with spin qubits in quantum dots into hybrid architectures⁶⁷⁻⁷⁷.

Most of the studies⁷⁷⁻⁸⁷ so far focused on the transport properties of such NWs in the topological regime or on properties of MFs themselves and their dependence on physical parameters. Also, there has been substantial interest recently in the investigation of the spin polarization of Andreev and Majorana bound states^{88,89}. However, it has been pointed out that great care must be taken when identifying topological phases from the presence of quasiparticle states inside the superconducting gap⁹⁰⁻⁹². Thus, it is most desirable to have additional signatures available (besides MFs) that would allow one to identify the topological phase transition. Re-

cent works, which analyzed the bulk signatures of the topological transition, focused either on the spinless Kitaev model⁹³ or studied finite-size scaling of the ground state energy in a generic conformal field theory approach for each of the symmetry classes⁹⁴. In this work, we would like to investigate the experimentally most relevant model of Rashba NWs and to provide relevant quantities accessible by state-of-the-art measurements. In contrast to aforementioned works, we also focus on local boundary effects and consider here different aspects of topological phases in one-dimensional systems, namely non-transport signatures of the topological phase transition in the *bulk* states, or, more precisely, in the boundary charge and boundary spin to which all occupied states close to the Fermi level contribute.

The paper is organized as follows. In Sec. II, we introduce the Rashba NW setup, which is modeled and analyzed in a tight-binding description by means of exact diagonalization, where all four components of the quasiparticle wavefunctions, needed for calculating the observables of interest, are obtained. In Sec. III, we focus on the boundary spin in the topological and trivial phases and find pronounced signatures in the spin component along the magnetic field direction, which allows us to identify the topological phase transition point. We summarize our results in Sec. IV.

II. MODEL

We investigate the system composed of a semiconducting NW with strong Rashba SOI in the proximity to a bulk *s*-wave superconductor in the presence of a magnetic field B applied along the NW axis along z direction, see Fig. 1. The SOI vector α points along the y direction. The B -field results in the Zeeman energy $\Delta_Z = g\mu_B B/2$, where g is g -factor and μ_B the Bohr magneton. The corresponding tight-binding Hamiltonian is written as⁸²

$$\begin{aligned}
 H = & -t \sum_{\langle jj' \rangle \sigma} \left(c_{j\sigma}^\dagger c_{j'\sigma} + \text{H.c.} \right) + (2t - \mu) \sum_{j\sigma} c_{j\sigma}^\dagger c_{j\sigma} \\
 & + \Delta_Z \sum_{j\sigma\sigma'} c_{j\sigma}^\dagger \sigma_z^{\sigma\sigma'} c_{j\sigma'} + i \sum_{\langle jj' \rangle \sigma\sigma'} \left(\alpha c_{j\sigma}^\dagger \sigma_y^{\sigma\sigma'} c_{j'\sigma'} + \text{H.c.} \right) \\
 & + \Delta_{SC} \sum_j \left(c_{j\uparrow}^\dagger c_{j\downarrow}^\dagger + \text{H.c.} \right), \quad (1)
 \end{aligned}$$

where the creation operator $c_{j\sigma}^\dagger$ creates an electron with spin $\sigma = \uparrow, \downarrow$ at site j of a chain consisting of N sites with lattice constant a . In the first and fourth terms, the summation runs only over neighbouring sites j and j' . Here, t denotes a nearest-neighbour hopping matrix element, μ is the chemical potential, and Δ_{SC} denotes the superconducting gap induced by proximity to the bulk *s*-wave superconductor. We note that in our model $\mu = 0$ corresponds the chemical potential being tuned to the SOI energy, which is defined here as $E_{SO} = \alpha^2/t$. For

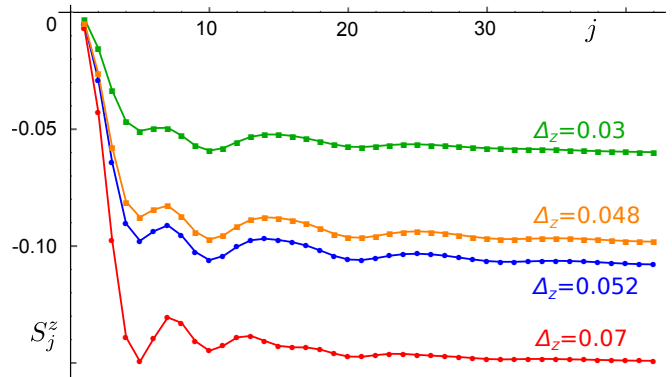


Figure 2. The spin density S_j^z (projection along \mathbf{B} -field) as a function of site j . Away from the NW ends, S_j^z is constant and given by S_0^z determined solely by bulk properties of the system. However, close to NW ends, S_j^z oscillates in all parameter regimes and there is no qualitative difference between trivial (indicated by squares) and topological (indicated by dots) phase. In all plots, the lines are guides to the eye. However, there is a quantitative shift in the amplitude of the first oscillations, as the system is driven through the topological phase as well as close to the topological phase transition in (blue, $\Delta_Z = 0.048$) and out of (orange, $\Delta_Z = 0.052$) the topological phase. The parameters are fixed to $N = 150$, $\mu = 0$, $\alpha = 0.3$, and $\Delta_{SC} = 0.05$. This choice of parameters corresponds to typical values observed in experiments with nanowires such as: $m = 0.015m_e$, $v_F = 0.8 \times 10^6$ m/s, $E_{SO} = 0.9$ meV, and $\Delta_{SC} = 0.5$ meV (with $a = 15$ nm, $t = 10$ meV).

the rest of the paper we fix $t = 1$ and use it as an energy scale. The system is in the topological phase hosting zero-energy MFs at the nanowire ends if $\Delta_Z > \Delta_Z^c$, where $\Delta_Z^c = \sqrt{\mu^2 + \Delta_{SC}^2}$ ^{42,43}. To study the topological phase transition in semiconducting NWs, we focus on the experimentally most relevant strong SOI regime, $E_{SO} \gg \Delta_{SC}, \Delta_Z$ ^{60,64}.

By diagonalizing numerically the Hamiltonian H [see Eq. (1)], one can determine the energy spectrum E_n . In addition, one also finds the operators $\psi_n = \sum_j \left(u_{\uparrow nj}^* c_{\uparrow j} + u_{\downarrow nj}^* c_{\downarrow j} + v_{\uparrow nj}^* c_{\uparrow j}^\dagger + v_{\downarrow nj}^* c_{\downarrow j}^\dagger \right)$, corresponding to annihilation operators for each of these $n = 4N$ states. Due to particle-hole symmetry, all states appear in pairs, *i.e.* if E_n is a solution, then so is $-E_n$. In what follows, we will focus on non-positive energy states. To characterize local bulk properties, we define the local charge ρ_j and the local spin densities $S_j^{x,y,z}$ at each site

as

$$\rho_j = \sum_{E_n < 0; \sigma} (|u_{\sigma nj}|^2 - |v_{\sigma nj}|^2), \quad (2a)$$

$$S_j^z = \sum_{E_n < 0; \sigma} \sigma (|u_{\sigma nj}|^2 - \sigma |v_{\sigma nj}|^2), \quad (2b)$$

$$S_j^x = \sum_{E_n < 0; \sigma} (u_{\sigma nj} u_{\bar{\sigma} nj}^* - v_{\sigma nj} v_{\bar{\sigma} nj}^*), \quad (2c)$$

$$S_j^y = i \sum_{E_n < 0; \sigma} (\sigma u_{\sigma nj} u_{\bar{\sigma} nj}^* - \sigma v_{\sigma nj} v_{\bar{\sigma} nj}^*), \quad (2d)$$

where the index $\sigma = 1$ ($\bar{1}$) corresponds also to spin up (down) states defined above, see Fig. 2. For zero-energy MF wavefunctions one can show that $u_{\uparrow nj}^* = v_{\uparrow nj}$ and $u_{\downarrow nj}^* = v_{\downarrow nj}$. Thus, the MF charge and spin densities are exactly zero⁹⁷ and they do not contribute to Eq. (2). For this reason, we take in our definition only bulk states with negative energies into account. In addition, in our model, the Hamiltonian is real, so all the eigenvectors can also be chosen to be real. As a consequence, we find that S^y is identically zero for all configurations considered below.

Away from the NW ends, both spin and charge densities are constant as expected in a translationally invariant system, see Fig. 2. However, close to the NW end, these quantities oscillate around their bulk values ρ_0 and $S_0^{x,z}$ determined as the value at the middle of the NW $\rho_0 = \rho_{j=\lfloor \frac{N}{2} \rfloor}$ and $S_0^{x,z} = S_{j=\lfloor \frac{N}{2} \rfloor}^{x,z}$, where $\lfloor M \rfloor$ denotes the integer part of M . Here, we assume that the NW is long enough such that these oscillations decay in the middle of the NW. In the strong SOI regime^{87,97}, there are two lengthscales associated with bulk gaps at exterior branches $\xi_e/a = 2\alpha/\Delta_{SC}$ and interior branches $\xi_i/a = 2\alpha/|\Delta_{SC} - \Delta_Z|$. In what follows, we work in the regime in which the NW length L is much longer than both ξ_e and ξ_i , see Fig. 2.

Our main interest are boundary effects. As a result, for further convenience⁹⁵, we define the left and right boundary charge and spin as

$$\tilde{\rho}_{Lm} = \sum_{j=1}^m (\rho_j - \rho_0), \quad (3)$$

$$\tilde{S}_{Lm}^{x,z} = \sum_{j=1}^m (S_j^{x,z} - S_0^{x,z}), \quad (4)$$

$$\tilde{\rho}_{Rm} = \sum_{j=N-m}^N (\rho_j - \rho_0), \quad (5)$$

$$\tilde{S}_{Rm}^{x,z} = \sum_{j=N-m}^N (S_j^{x,z} - S_0^{x,z}). \quad (6)$$

First, we subtract from charge and spin densities their bulk values. Second, we sum densities over m sites at the left or right edge to define the right and left boundary charge or spin. Our system is symmetric with respect to the middle of the NW, so right and left boundary charges

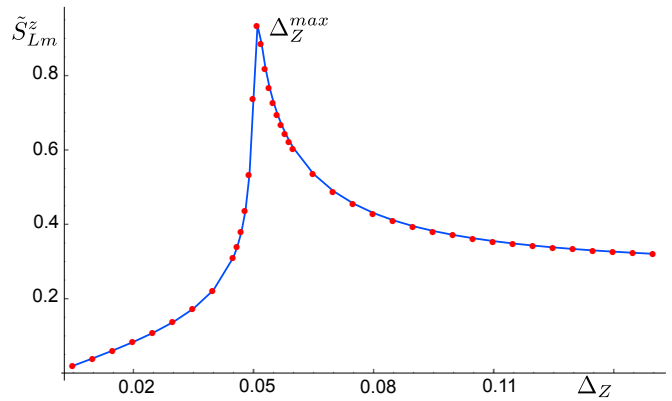


Figure 3. The left boundary spin component along z direction, \tilde{S}_{Lm}^z , [see Eq. (4)] as a function of the Zeeman energy Δ_Z . The \tilde{S}_{Lm}^z has a peak at Δ_Z^{max} , which coincides in sufficiently long systems with the point of the topological phase transition $\Delta_Z = \Delta_{SC}$. This peak is an independent signature of the topological phase transition. The system parameters are taken to be $\alpha = 0.3$, $\Delta_{SC} = 0.05$, $\mu = 0$, $N = 2000$, and $m = 1000$.

and spins can at most differ in sign. In our case, we find that $\tilde{\rho}_{Lm} = \tilde{\rho}_{Rm}$ and $\tilde{S}_{Lm}^z = \tilde{S}_{Rm}^z$, whereas $\tilde{S}_{Lm}^x = -\tilde{S}_{Rm}^x$, see the Appendix A. We confirm that for values of m such that $\max\{\xi_e, \xi_i\}/a \ll m \ll N/2$, $\tilde{\rho}_m$ and $\tilde{S}_m^{x,z}$ converge to a constant values $\tilde{\rho}_{R,L}$ and $\tilde{S}_{R,L}^{x,z}$. Without loss of generality, in what follows, we focus only on the left boundary charge and spin.

III. SIGNATURE OF TOPOLOGICAL PHASE TRANSITION

Next, we focus on the characteristic behavior of the boundary charge and spin around the topological phase transition. First, we analyze the behaviour of the spin density along the magnetic field S_j^z for various values of Zeeman gaps and all the other parameters fixed, see Fig. 2. As expected, S_j^z is constant in the middle of the chain and saturates to S_0^z , however, as one approaches the end of the chain, spatial oscillations in S_j^z begin to emerge. Not surprisingly, the spin polarization along the magnetic field strongly depends on the strength of the B -field. The stronger the magnetic field is, the larger is the polarization, see Fig. 2. Close to the phase transition point, the oscillations in S_j^z at the NW ends get more pronounced and are characterized by higher amplitudes and longer decay lengths. In order to quantify these oscillations, we calculate numerically the boundary spin and charge as defined in Eq. (4). The signature of the topological phase transition can be clearly seen in the z -component of the boundary spin, $S_{L/Rm}^z$, see Fig. 3. In the Appendix A, we also provide details on the boundary charge and the S^x -component, however, there is no signature of the topological phase transition in these quantities. In contrast to that, the $S_{L/Rm}^z$ has a pronounced

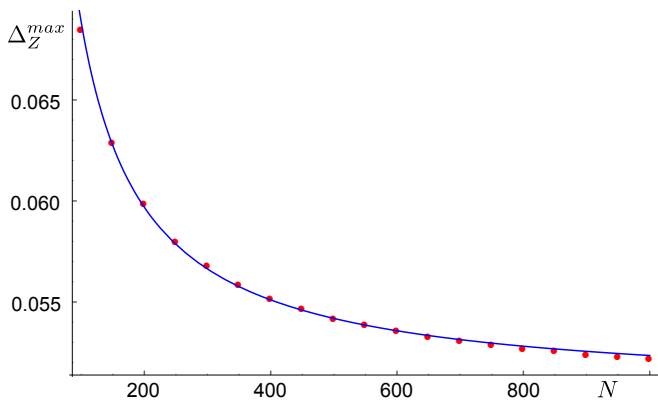


Figure 4. The position of the peak Δ_Z^{max} in \tilde{S}_{Lm}^z [see Eq. (4)] as a function of system size N . As the system size is increases, Δ_Z^{max} gets more and more close to the critical value Δ_Z^c at which the topological phase transition takes place. We find that the obtained numerically results (red dots) can be fitted the best with the analytical formula $(\Delta_Z^{max} - \Delta_Z^c) \propto 1/N$ (blue curve). The system parameters are the same as in Fig. 3 with $m = N/2$.

peak at the value of the Zeeman energy Δ_Z^{max} that is very close to the critical value Δ_Z^c determined from the topological criterion. The longer the system is, the more close Δ_Z^{max} to Δ_Z^c , see Fig. 4. We find that Δ_Z^{max} weakly depends on the system size N and approaches the critical value asymptotically as a function of $1/N$. Importantly, the value of $S_{L/Rm}^z$ does not depend on whether the MF state is occupied or not as its contribution is identically zero. Thus, for long enough systems, the position of the peak in $S_{L/Rm}^z$ can be used as an independent signature of the topological phase transition.

It is also important to emphasize the role of the chemical potential μ . It is well known that the system can also be driven between topological and trivial phases by changing μ ^{42,43}. In this case, when the topological phase is reached, there are two peaks in \tilde{S}_{Lm}^z at two critical values $\mu = \pm\mu^c$ with $\mu^c = \sqrt{\Delta_Z^2 - \Delta_{SC}^2}$, see Fig. 5. Again, we see that the critical values $\pm\mu^c$ are asymptotically reached as the size of the system is increased. However, when the width of two peaks is comparable with μ^c , the two peaks will merge. Thus, this criterion works best for large values of Δ_Z and long systems. We note that one faces the same problem if the detection of the phase transition is done via zero-bias peak signatures in transport measurements. In short nanowires, the MFs of opposite ends will overlap and split away from zero energy if one is not deeply in the topological phase.

Finally, we would like to demonstrate the stability of the presented signatures against disorder and, thus, show that they are also topologically protected. For this, we add on-site disorder to our model [see Eq. (1)] as well as we modify the system by adding trivial section at the NW end. Results for the both cases are presented in the Appendices C, D. In all configurations, the signature of the topological phase transition in the boundary spin

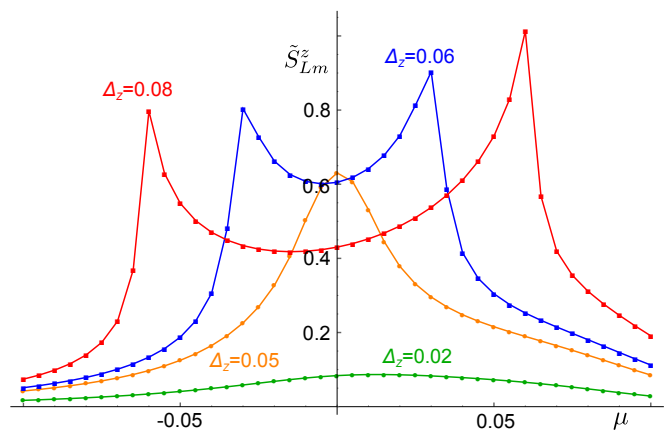


Figure 5. The z component of the boundary spin \tilde{S}_{Lm}^z [see Eq. (4)] as a function of the chemical potential μ . In the topological regime, there are two peaks corresponding to two critical values of the chemical potential $\pm\mu^c$, at which the system goes through the topological phase transition. In the trivial regime such peaks are absent as the system cannot be tuned into the topological phase. Far from the transition point (green, $\Delta_Z = 0.02$) there is a broad maximum in \tilde{S}_{Lm}^z which gets more pronounced as system approaches the topological phase transition (orange, $\Delta_Z = 0.05$) and develops later into a double peak structure (blue, $\Delta_Z = 0.06$ and red, $\Delta_Z = 0.08$) in the topological phase. The system parameters are fixed to $N = 1000$, $\alpha = 0.3$, $\Delta_{SC} = 0.05$, and $m = 500$.

\tilde{S}_{Lm}^z is still fully present.

So far we have focused on signatures of the topological phase transition to be detected in the boundary spin. However, the bulk values of the spin component along the magnetic field S_0^z also carry information about the topological phase transition if periodic boundary conditions are imposed, see the Appendix E for details. In this case, the system is translationally invariant and it does not matter at which point one computes the bulk value of the spin component S_{PBC}^z . The signature of the topological phase transition is still present but different. In particular, there is now a sharp discontinuity in S_{PBC}^z with a jump of order $1/N$ at the point of the topological phase transition, $\Delta_Z = \Delta_Z^c$, see the Appendix E.

The measurement of boundary spins will be challenging but seems to be within reach for state-of-the-art magnetometry with NV-centers or nanoSQUIDS^{98–103}. We furthermore recall that it is the total integral over the spin density within the localization length that determines the spin signature of the phase transition. Thus, a resolution of the measurement device over this length scale should be sufficient and is already reached in the aforementioned magnetometric measurements. Moreover, all those techniques were already performed at cryogenic temperatures necessary for our proposal as one should work at temperatures that do not exceed the scale set by the bulk gap⁹⁶. Finally, in contrast to STM measurements, these techniques are non-invasive and, thus, can be used to measure reliably the magnetic signals we

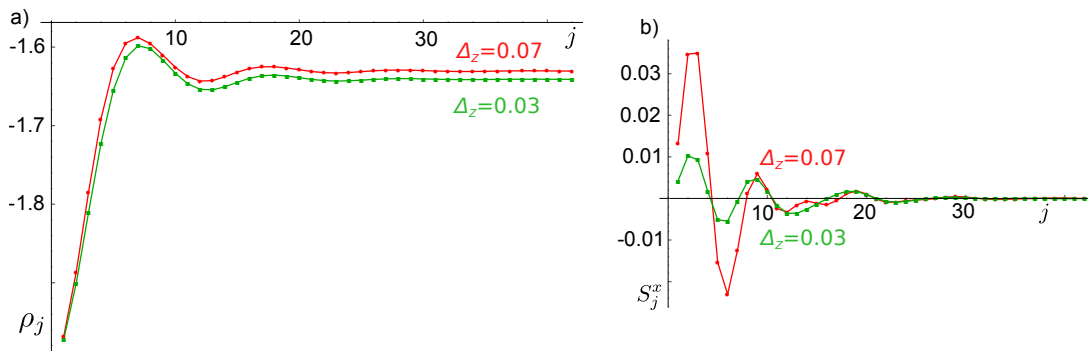


Figure 6. (a) Charge density ρ_j and (b) component of the spin density along the x axis, S_j^x , as a function of site position j . The characteristic features are similar to those of S_j^z discussed in the main text, again there are oscillations close to the NW ends in both trivial and topological phases. However, neither the amplitude of the first oscillation does not differ between the two phases [see (a)] nor the oscillations tend to cancel each other [see (b)]. Results for the trivial (topological) phase are marked by green squares (red cycles) and correspond to $\Delta_Z = 0.03$ ($\Delta_Z = 0.07$). The system parameters are chosen to be $N = 150$, $\mu = 0$, $\alpha = 0.3$, $\Delta_{SC} = 0.05$.

propose.

IV. CONCLUSIONS

We have identified signatures of the topological phase transition in the boundary spin component in one-dimensional topological systems. These signatures are present when tuning through the phase transition point either with the magnetic field or with the chemical potential. Moreover, we have shown that these signatures do not rely on the presence of MFs and always occur at the boundary between topological and trivial sections of the NW. We have analyzed the finite-size effects of the boundary spin and shown that the position of the peak

converges to the value obtained analytically in the continuum limit. These results are also stable with respect to disorder.

ACKNOWLEDGMENTS

We are grateful to S. Hoffman, P. Szumniak and D. Chevallier for valuable discussions. We acknowledge support by the Swiss National Science Foundation and the NCCR QSIT. This project has received funding from the European Union's Horizon 2020 research and innovation program (ERC Starting Grant, grant agreement No 757725).

Appendix A: Results for boundary spin component S_{Lm}^x and boundary charge ρ_{Lm}

For the sake of completeness, we present here our results for the local spin density S_j^x and charge density ρ_j , see Fig. 6. As the SOI vector points along the x direction, it is expected that S_j^x in the center of the chain vanishes and moreover $\sum_{j=1}^N S_j^x = 0$, which imposes that S_j^x must be antisymmetric with respect to the middle of the chain. We confirm this expectation by exact numerical diagonalization. As in the case of S_j^z , spatial oscillations in S_j^x appear close to the ends of the NW, get-

ting more pronounced as one approaches the topological phase transition. In case of the charge density ρ_j , the characteristic behavior is very similar while in this case, as expected, the results are symmetric with respect to the middle of the wire. We also calculate the corresponding boundary charge $\tilde{\rho}_{Lm}$ and the boundary spin component \tilde{S}_{Lm}^x (see Fig. 7). However, we do not observe any well-pronounced signatures of the topological phase transition in these quantities. For $\tilde{\rho}_{Lm}$, we can see a transition from almost constant to a linear dependence of Δ_Z , however, this signature seems to be difficult to measure.

Appendix B: Local properties of boundary spin component \tilde{S}_{Lm}^z

We would like to elaborate on the question in which sense \tilde{S}_{Lm}^z is a *local* signature emerging only at the end of the NW. In other words, we should investigate the behavior of \tilde{S}_{Lm}^z with respect to changes in m , see Fig. 8.

Far from the topological phase transition, we observe that \tilde{S}_{Lm}^z converges very quickly with increasing m and is therefore a local property of the end of the NW. As we approach the transition point, values for the respective m 's start to differ. Nevertheless, even for $m = 20$ we still observe a well-pronounced peak almost at the same Δ_Z as for $m = 100$. Based on that we can conclude that \tilde{S}_{Lm}^z

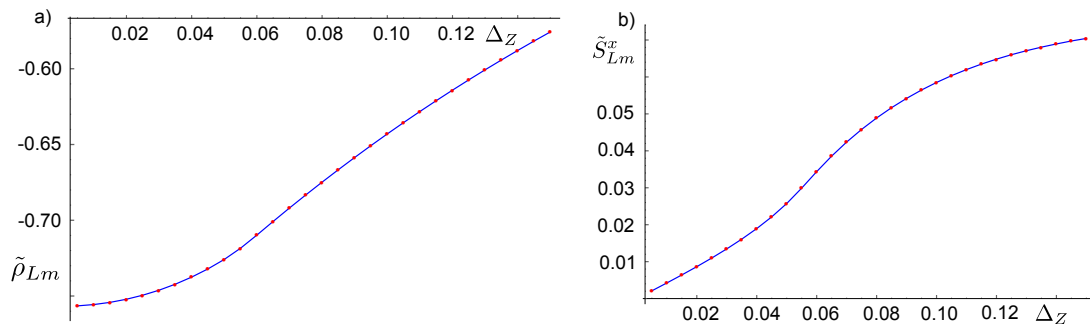


Figure 7. (a) Boundary charge $\tilde{\rho}_{Lm}$ and (b) component of the boundary spin along the x axis \tilde{S}_{Lm}^x as a function of Zeeman energy Δ_Z . There are only weak features associated with the topological phase transition. Unlike the pronounced peak in \tilde{S}_{Lm}^z , the component \tilde{S}_{Lm}^x cannot reliably distinguish the trivial from topological phase. The system parameters are chosen to be $\alpha = 0.3$, $\Delta_{SC} = 0.05$, $\mu = 0$, $N = 200$, and $m = 100$.

is a local quantity with main support at the end of the NW.

For completeness, we also show that the signature of the topological phase transition in \tilde{S}_{Lm}^z does not crucially depend on a large value of the SOI strength, see Fig. 9. Indeed, the peak is even more pronounced in the regime of weak SOI.

Appendix C: Effect of on-site disorder - stability of topological phase transition signature in \tilde{S}_{Lm}^z

To demonstrate that the presented signature of the topological phase transition in the boundary spin component \tilde{S}_{Lm}^z is robust, we must verify that this signature persists even if the disorder is present, see Fig. 10.

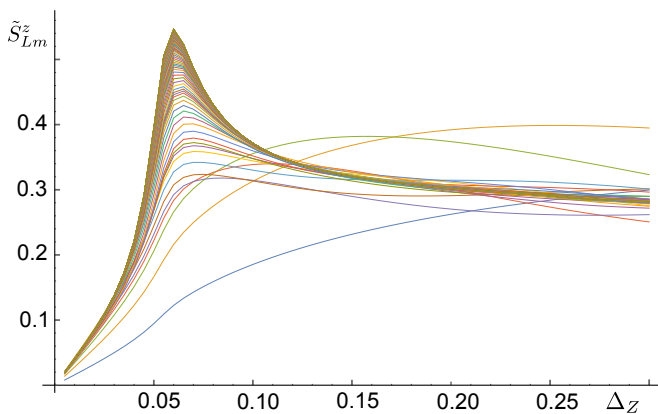


Figure 8. Component of the boundary spin along z axis, \tilde{S}_{Lm}^z , [see Eq. (4)] as a function of Zeeman energy Δ_Z for different cut-off values: $m = 1, \dots, 100$. Here, $m = 1$ corresponds to the lowest blue curve. Other curves are ordered according to ascending m at small Δ_Z . The peak in \tilde{S}_{Lm}^z close to Δ_Z^c is observed already for $m = \xi_{SC}/a$ ($\xi_{SC}/a = 12$ for this plot), thus, the proposed signature of the topological phase transition is local with contributions coming from the occupied bulk states at the end of the NW. The system parameters are chosen to be $N = 200$, $\alpha = 0.3$, $\Delta_{SC} = 0.05$, and $\mu = 0$.

We perform the same calculations as before, however, add fluctuations in the chemical potential. We see that, locally, disorder causes the appearance of a similar feature in the spin density as already observed at the NW ends. Namely, there is a local maximum in the spin density S_j^z at the position of the impurity. The oscillations around the impurity position decay as one moves away. If there are many impurities, such effects will average out. As a result, there can be only local redistribution of the spin density S_j^z , which do not affect the boundary spin \tilde{S}_{Lm}^z . Therefore, as expected, the signature of the topological phase transition, *i.e.* peak in \tilde{S}_{Lm}^z at Δ_Z^c , is robust against local disorder. This holds also in the case of disorder as strong as the superconducting gap Δ_{SC} itself and well beyond.

Next, we add magnetic disorder. A magnetic impurity at site j pointing in arbitrary direction defined by two

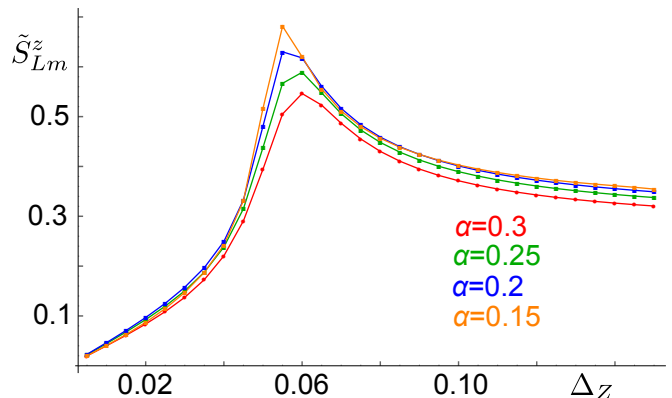


Figure 9. Component of the boundary spin along z axis, \tilde{S}_{Lm}^z , [see Eq. (4)] as a function of Zeeman energy Δ_Z for different values of SOI. We compare the experimentally relevant regime of strong SOI (red), $\alpha = 0.3$, with intermediate SOI regimes, $\alpha = 0.25$ (green) and $\alpha = 0.2$ (blue), as well as with weak SOI regime, $\alpha = 0.15$ (orange). The peak gets even more pronounced as one tunes from strong to weak SOI regime. The system parameters are chosen to be $N = 200$, $\Delta_{SC} = 0.05$, $m = 100$ and $\mu = 0$.

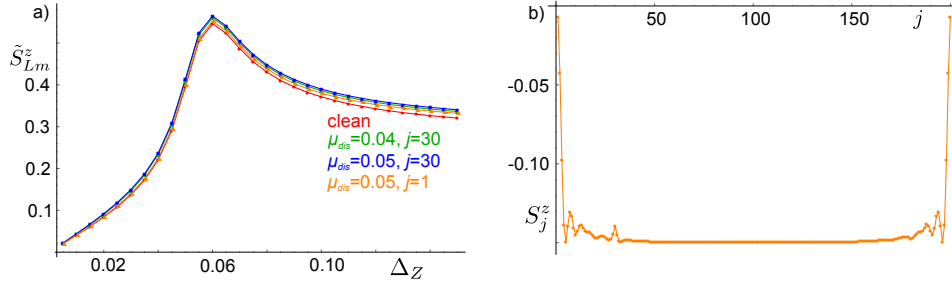


Figure 10. (a) Component of the boundary spin, \tilde{S}_{Lm}^z , and (b) the z -component of the local spin density S_j^z in the system with on-site potential disorder. Generally, we observe the same behavior as in the clean case, accompanied by small overall renormalization of \tilde{S}_j^z even in the case of relatively strong disorder. We add disorder in the chemical potential μ_{dis} on site j , elsewhere, we keep $\mu = 0$. In panel (a), \tilde{S}_{Lm}^z for the clean wire (red) is compared with results for a disordered wire with $\mu_{dis} = 0.04$ at site $j = 30$ (green); with $\mu_{dis} = 0.05$ at site $j = 30$ (blue); and with $\mu_{dis} = 0.04$ at site $j = 1$ (orange). If an impurity located at the first site of the NW, the boundary spin is left unchanged even for very strong values of disorder, $\mu_{dis} = 0.1$. The signature of the topological phase transition is clearly not affected by disorder. In panel (b), S_j^z is shown for a disordered NW with $\mu_{dis} = 0.04$ at site $j = 30$ ($\Delta_Z = 0.07$). The presence of the impurity manifests itself as an additional local peak in S_j^z accompanied by spatial oscillations. As a result, there is a local redistribution of the spin density, which does not affect the boundary spin. If there are several impurities, their contributions average out and the system gets even more stable to disorder. The system parameters are chosen to be $N = 200$, $\alpha = 0.3$, $\Delta_{SC} = 0.05$, and $m = 100$.

spherical angles (θ, ϕ) is modeled by adding the following term to the total Hamiltonian H ,

$$H_{MI,j} = J \sum_{\sigma, \sigma'} c_{j\sigma}^\dagger \left(\sin \theta \cos \phi \sigma_x^{\sigma\sigma'} + \sin \theta \sin \phi \sigma_y^{\sigma\sigma'} + \cos \theta \sigma_z^{\sigma\sigma'} \right) c_{j\sigma'}. \quad (C1)$$

We repeat the same procedure as described before for potential disorder and again compare the results with the case of the clean wire, see Fig. 11. In case of a magnetic impurity pointing in the z direction along (opposite to) the direction of magnetic field, there is a dip (peak) in the local spin density. Such an effective local magnetic field sums up with the externally applied uniform field and increases (decreases) the total spin polarization, and,

thus, affects the height but not the position of the peak in the boundary spin. In the case of the magnetic impurity pointing along the x direction, there is a peak in the local spin density. This can be understood as follows: the local magnetic field polarizes spins locally along the x direction, and, thus, diminishes the polarization in the z direction, resulting in a local peak. In the case of a magnetic impurity pointing along the y direction, there are practically no changes in the local spin density of states nor in the boundary spin. If the magnetic impurity is far away from the boundary, there is no effect on the boundary spin. In case of multiple magnetic impurities such effects average out. To conclude, magnetic disorder does not affect the signature of the topological phase transition carried by the boundary spin.

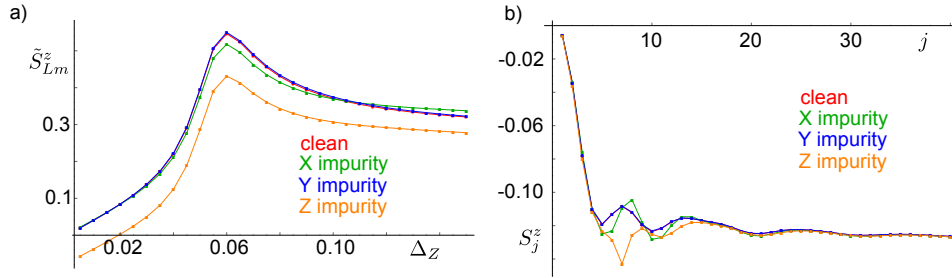


Figure 11. (a) Component of the boundary spin, \tilde{S}_{Lm}^z , and (b) the z -component of the local spin density S_j^z in the presence of on-site magnetic disorder. Generally, we observe the same behavior as in the clean case accompanied by small overall renormalization of \tilde{S}_{Lm}^z . (a) Boundary spin \tilde{S}_{Lm}^z for the clean wire (red) is compared with results for a disordered wire with a magnetic impurity of the strength $J = 0.05$ placed at site $j = 7$ in different configurations: polarization along the x direction (green) with $\theta = \pi/2$, $\phi = 0$; polarization along the y direction (blue) with $\theta = \pi/2$, $\phi = \pi/2$; polarization along the z direction (orange) with $\theta = 0$. (b) Close to the magnetic impurity, the local spin density S_j^z is changed, resulting in either an increase or decrease in the local spin polarization ($\Delta_Z = 0.06$). This local redistribution of the spin density hardly affects the boundary spin and does not obscure the signature of the topological phase transition. If there are several magnetic impurities, their contributions average out. The system parameters are chosen to be $N = 200$, $\alpha = 0.3$, $\Delta_{SC} = 0.05$, and $m = 100$ if not specified otherwise.

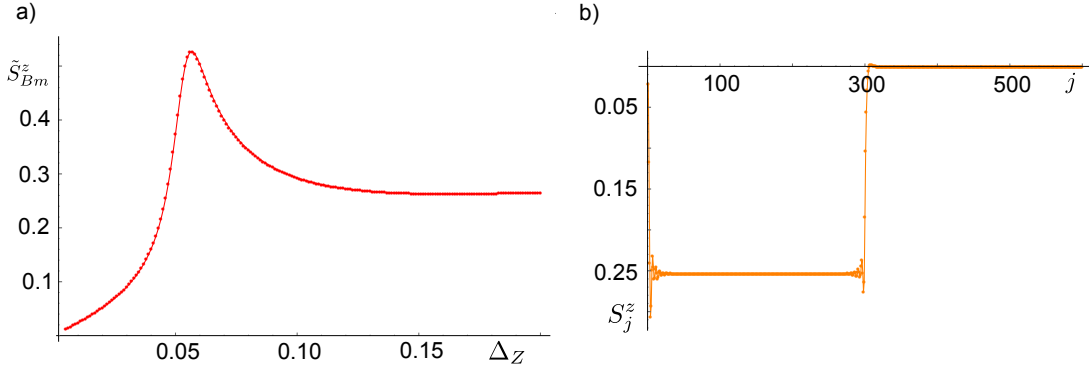


Figure 12. (a) Component of the boundary spin, \tilde{S}_{Bm}^z , and (b) the z -component of the local spin density S_j^z . The right section of the NW corresponds to a superconducting lead, in which we fix $\alpha = \Delta_Z = 0$. In contrast to that, the left section of the NW is described by $\alpha = 0.3$. The chemical potential is uniform, $\mu = 0$, as well as the superconducting strength $\Delta_{SC} = 0.05$. In addition, $N_< = N_> = 300$ and $m_< = m_> = 150$. (a) Again, there is a signature of the topological phase transition in \tilde{S}_{Bm}^z . (b) The boundary spin has contributions from both topological and trivial sections of the NW ($\Delta_Z = 0.15$). We also note that the bulk values of spin density S_j^z are different in two sections.

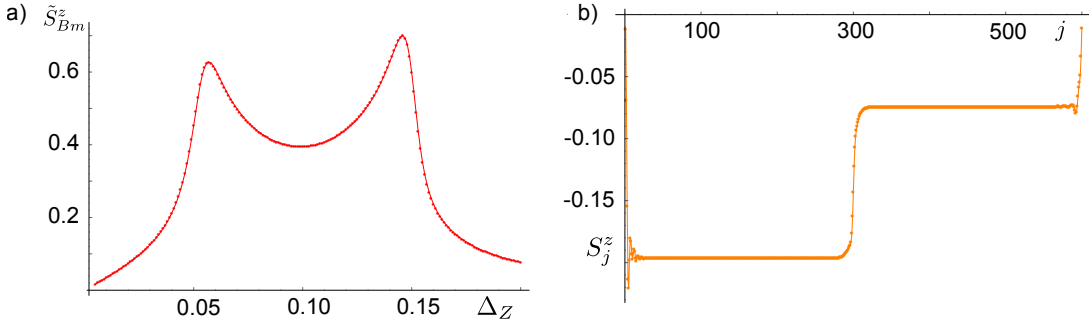


Figure 13. The same as in Fig. 12, however, here, both sections of the NW have the same strength of the SOI ($\alpha = 0.3$) and the same strength of Zeeman energy. However, the proximity-gap is non-uniform: *i.e.* the right (left) section has $\Delta_{SC} = 0.15$ ($\Delta_{SC} = 0.05$). As a result, in panel (a), there are two peaks in \tilde{S}_{Bm}^z , which corresponds to two values at which each of sections changes from the trivial to the topological phase. (b) The z -component of the local spin density S_j^z saturates at two different values at the left and right sections, which motivates us to introduce $S_{0<}^z$ and $S_{0>}^z$ for each section separately ($\Delta_Z = 0.10$).

Appendix D: Boundary spin \tilde{S}_{Rm}^z at the boundary between topological and trivial phases

In the main text, we have focused on the boundary spin located at the ends of the NW. Here, we show that, generally, the boundary spin is associated with the boundary between topological and trivial sections in the NW. As a result, there is a contribution to $\tilde{S}_{L/Rm}^z$ coming from both sides of the boundary, *i.e.* from the topological section and from the trivial section. This means that the definitions for $\tilde{S}_{R/Lm}^z$ given by Eqs. (4) and (6) should be generalized. For the moment, let us focus on the boundary spin located at the site N and introduce the boundary spin as

$$\begin{aligned} \tilde{S}_{Bm}^z &= \sum_{j=N-m_<}^N (S_j^z - S_{0<}^z) - \sum_{j=N+1}^{N+m_>} (S_j^z - S_{0>}^z), \\ S_{0<}^z &= S_{j=[\frac{N_<}{2}]}^z, \quad S_{0>}^z = S_{j=[N_< + \frac{N_>}{2}]}^z. \end{aligned} \quad (\text{D1})$$

Here, the sum runs over $m_<$ ($m_>$) sites of the left (right) section of the NW consisting in total of $N_<$ ($N_>$) sites, such that $m = m_< + m_>$. Without loss of generality, we can assume that the left (right) section is in the topological (trivial) phase. Assuming that both sections are long enough, one determines the bulk value of the spin density as $S_{0<}^z$ and $S_{0>}^z$ for each section separately, as they are generally not the same. This can be seen clearly in Figs. 13(b) and 12(b), where we show how a typical spin density profile looks like in NWs divided into two sections.

We consider two scenarios. In the first scenario (see Fig. 12), we attach a superconducting lead at the right end of the NW. In this lead, we assume that the Zeeman field is screened and the SOI is absent. As a result, this NW section is always in the trivial phase. Again, one observes a well-pronounced peak in \tilde{S}_{Bm}^z at Zeeman energies close to the critical value Δ_Z^c . In the second scenario (see Fig. 13), the right section of the NW has stronger proximity-induced superconductivity. Thus, it enters the topological phase at larger values of Zeeman

energy. As a result, there are two peaks in \tilde{S}_{Bm}^z . The first (second) peak corresponds to a Zeeman energy at which left (right) section of the NW becomes topological.

Appendix E: Signatures of topological phase transition in bulk values of spin

So far we have focused on signatures of the topological phase transition to be detected in the boundary spin. However, the bulk values of the spin polarization along the magnetic field, S_0^z , also carries the information about the phase transition in finite-size systems. To focus on bulk properties only and to exclude any influence of boundary effects, we impose now periodic boundary conditions on the system, forming a NW ring. In this case the system is translationally invariant and it does not matter at which point one computes the bulk value

of the spin polarization S_{PBC}^z . In finite-size systems, we always observe a sharp discontinuity in S_{PBC}^z at the point of the topological phase transition, $\Delta_Z = \Delta_Z^c$, see Fig. 14. In contrast to the boundary spin, this discontinuity always takes place at Δ_Z^c independent of the system size. However, the value of the jump ΔS_{PBC}^z in S_{PBC}^z depends on the size of the system. We analyzed the value of the jump as a function of system size N and conclude that it can be fitted best by an $1/N$ dependence. We note that the results of this subsection obtained for bulk states with periodic boundary conditions are closely related to the ones obtained for bulk states in Ref. 31. In particular, the sign reversal of the spin polarization of the bulk state with zero momentum is responsible for the jump in S_{PBC}^z . In stark contrast, the features of the boundary spin \tilde{S}_{Bm}^z are due to boundary effects and thus are of different physical origin.

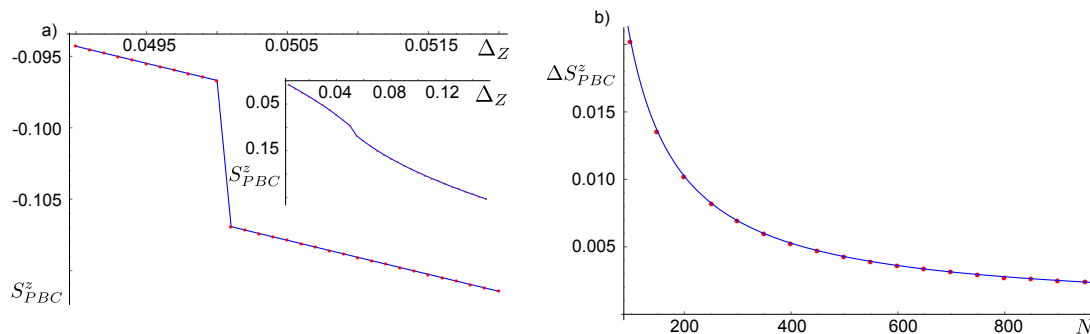


Figure 14. (a) Component of spin polarization along the z axis, S_{PBC}^z , as a function of Zeeman energy in the system with periodic boundary conditions. Away from the topological phase transition point Δ_Z^c , S_{PBC}^z is a linear function of Δ_Z . The discontinuity in spin polarization, ΔS_{PBC}^z , occurs exactly at Δ_Z^c . (b) The size of the jump ΔS_{PBC}^z is inversely proportional to the system size N . Numerical results (red dots) are fitted by the analytical formula $\Delta S_{PBC}^z \propto 1/N$ (blue curve). The system parameters are chosen to be $\alpha = 0.3$, $\Delta_{SC} = 0.05$, $\mu = 0$, and $m = N/2$

-
- ¹ W. P. Su, J. R. Schrieffer, and A. J. Heeger, Phys. Rev. Lett. **42**, 1698 (1979).
 - ² W. P. Su and J. R. Schrieffer, Phys. Rev. Lett. **46**, 738 (1981).
 - ³ J. Goldstone and F. Wilczek, Phys. Rev. Lett. **47**, 986 (1981).
 - ⁴ R. Jackiw and C. Rebbi, Phys. Rev. D **13**, 3398 (1976).
 - ⁵ R. Jackiw and J. Schrieffer, Nuclear Physics B **190**, 253 (1981).
 - ⁶ W. P. Su and J. R. Schrieffer, Phys. Rev. Lett. **46**, 738 (1981).
 - ⁷ M. J. Rice and E. J. Mele, Phys. Rev. Lett. **49**, 1455 (1982).
 - ⁸ R. Jackiw and G. Semenoff, Phys. Rev. Lett. **50**, 439 (1983).
 - ⁹ S. Kivelson, Phys. Rev. B **28**, 2653 (1983).
 - ¹⁰ X.-L. Qi, T. L. Hughes, and S.-C. Zhang, Nature Physics **4**, 273 (2008).
 - ¹¹ N. Goldman, I. Satija, P. Nikolic, A. Bermudez, M. A. Martin-Delgado, M. Lewenstein, and I. B. Spielman, Phys. Rev. Lett. **105**, 255302 (2010).
 - ¹² S. Gangadharaiah, L. Trifunovic, and D. Loss, Phys. Rev. Lett. **108**, 136803 (2012).
 - ¹³ Y. E. Kraus, Y. Lahini, Z. Ringel, M. Verbin, and O. Zeitlinger, Phys. Rev. Lett. **109**, 106402 (2012).
 - ¹⁴ J. Klinovaja, P. Stano, and D. Loss, Phys. Rev. Lett. **109**, 236801 (2012).
 - ¹⁵ J. C. Budich and E. Ardonne, Phys. Rev. B **88**, 035139 (2013).
 - ¹⁶ Z. Xu, L. Li, and S. Chen, Phys. Rev. Lett. **110**, 215301 (2013).
 - ¹⁷ F. Grusdt, M. Hönig, and M. Fleischhauer, Phys. Rev. Lett. **110**, 260405 (2013).
 - ¹⁸ J. Klinovaja and D. Loss, Phys. Rev. Lett. **110**, 126402 (2013).
 - ¹⁹ K. A. Madsen, E. J. Bergholtz, and P. W. Brouwer, Phys. Rev. B **88**, 125118 (2013).
 - ²⁰ A. V. Poshakinskiy, A. N. Poddubny, L. Piloizzi, and E. L. Ivchenko, Phys. Rev. Lett. **112**, 107403 (2014).

- ²¹ D. Rainis, A. Saha, J. Klinovaja, L. Trifunovic, and D. Loss, Phys. Rev. Lett. **112**, 196803 (2014).
- ²² J. Klinovaja and D. Loss, Phys. Rev. Lett. **112**, 246403 (2014).
- ²³ R. Wakatsuki, M. Ezawa, Y. Tanaka, and N. Nagaosa, Phys. Rev. B **90**, 014505 (2014).
- ²⁴ P. Marra, R. Citro, and C. Ortix, Phys. Rev. B **91**, 125411 (2015).
- ²⁵ J. Klinovaja and D. Loss, The European Physical Journal B **88**, 62 (2015).
- ²⁶ G. van Miert and C. Ortix, Phys. Rev. B **96**, 235130 (2017).
- ²⁷ B. Pérez-González, M. Bello, A. Gómez-León, and G. Platero, arXiv:1802.03973.
- ²⁸ S. Ryu, C. Mudry, C. Hou, and C. Chamon, Phys. Rev. B **80**, 205319 (2009).
- ²⁹ B. Seradjeh, C. Weeks, and M. Franz, Phys. Rev. B **77**, 033104 (2008).
- ³⁰ A. Rüegg and G. A. Fiete, Phys. Rev. B **83**, 165118 (2011).
- ³¹ P. Szumniak, J. Klinovaja, and D. Loss, Phys. Rev. B **93**, 245308 (2016).
- ³² E. Majorana, Nuovo Cimento **14**, 171 (1937).
- ³³ B. A. Volkov and O. Pankratov, Pi'sma Zh. Eksp. Teor. Fiz. **42**, 145 (1985).
- ³⁴ B. A. Bernevig, T. L. Hughes, and S.-C. Zhang, Science **314**, 1757 (2006).
- ³⁵ M. König, S. Wiedmann, C. Brüne, A. Roth, H. Buhmann, L. W. Molenkamp, X.-L. Qi, and S.-C. Zhang, Science **318**, 766 (2007).
- ³⁶ L. Fu, C. L. Kane, and E. J. Mele, Phys. Rev. Lett. **98**, 106803 (2007).
- ³⁷ A. Roth, C. Brüne, H. Buhmann, L. W. Molenkamp, J. Maciejko, X.-L. Qi, and S.-C. Zhang, Science **325**, 294 (2009).
- ³⁸ M. Z. Hasan and C. L. Kane, Rev. Mod. Phys. **82**, 3045 (2010).
- ³⁹ T. A. Bernevig and T. L. Hughes, *Topological Insulators and Topological Superconductors* (Princeton University Press, 2013).
- ⁴⁰ L. Fu and C. L. Kane, Phys. Rev. Lett. **100**, 096407 (2008).
- ⁴¹ M. Sato and S. Fujimoto, Phys. Rev. B **79**, 094504 (2009).
- ⁴² R. M. Lutchyn, J. D. Sau, and S. Das Sarma, Phys. Rev. Lett. **105**, 077001 (2010).
- ⁴³ Y. Oreg, G. Refael, and F. von Oppen, Phys. Rev. Lett. **105**, 177002 (2010).
- ⁴⁴ J. Alicea, Phys. Rev. B **81**, 125318 (2010).
- ⁴⁵ A. C. Potter and P. A. Lee, Phys. Rev. B **83**, 094525 (2011).
- ⁴⁶ J. Klinovaja, S. Gangadharaiah, and D. Loss, Phys. Rev. Lett. **108**, 196804 (2012).
- ⁴⁷ D. Chevallier, D. Sticlet, P. Simon, and C. Bena, Phys. Rev. B **85**, 235307 (2012).
- ⁴⁸ S. Nadj-Perge, I. K. Drozdov, B. A. Bernevig, and A. Yazdani, Phys. Rev. B **88**, 020407 (2013).
- ⁴⁹ F. Pientka, L. I. Glazman, and F. von Oppen, Phys. Rev. B **88**, 155420 (2013).
- ⁵⁰ J. Klinovaja, P. Stano, A. Yazdani, and D. Loss, Phys. Rev. Lett. **111**, 186805 (2013).
- ⁵¹ B. Braunecker and P. Simon, Phys. Rev. Lett. **111**, 147202 (2013).
- ⁵² M. M. Vazifeh and M. Franz, Phys. Rev. Lett. **111**, 206802 (2013).
- ⁵³ M. Thakurathi, A. A. Patel, D. Sen, and A. Dutta, Phys. Rev. B **88**, 155133 (2013).
- ⁵⁴ F. Maier, J. Klinovaja, and D. Loss, Phys. Rev. B **90**, 195421 (2014).
- ⁵⁵ F. Setiawan, K. Sengupta, I. B. Spielman, and J. D. Sau, Phys. Rev. Lett. **115**, 190401 (2015).
- ⁵⁶ G. L. Fatin, A. Matos-Abiague, B. Scharf, and I. Žutić, Phys. Rev. Lett. **117**, 077002 (2016).
- ⁵⁷ S. Nadj-Perge, I. K. Drozdov, J. Li, H. Chen, S. Jeon, J. Seo, A. H. MacDonald, B. A. Bernevig, and A. Yazdani, Science **346**, 602 (2014).
- ⁵⁸ M. Ruby, F. Pientka, Y. Peng, F. von Oppen, B. W. Heinrich, and K. J. Franke, Phys. Rev. Lett. **115**, 197204 (2015).
- ⁵⁹ R. Pawlak, M. Kisiel, J. Klinovaja, T. Meier, S. Kawai, T. Glatzel, D. Loss, and E. Meyer, Npj Quantum Information **2**, 16035 (2016).
- ⁶⁰ V. Mourik, K. Zuo, S. M. Frolov, S. R. Plissard, E. P. A. M. Bakkers, and L. P. Kouwenhoven, Science **336**, 1003 (2012).
- ⁶¹ A. Das, Y. Ronen, Y. Most, Y. Oreg, M. Heiblum, and H. Shtrikman, Nature Physics **8**, 887 (2012).
- ⁶² L. P. Rokhinson, X. Liu, and J. K. Furdyna, Nature Physics **8**, 795 (2012).
- ⁶³ H. O. H. Churchill, V. Fatemi, K. Grove-Rasmussen, M. T. Deng, P. Caroff, H. Q. Xu, and C. M. Marcus, Phys. Rev. B **87**, 241401 (2013).
- ⁶⁴ S. M. Albrecht, A. P. Higginbotham, M. Madsen, F. Kuemmeth, T. S. Jespersen, J. Nygård, P. Krogstrup, and C. M. Marcus, Nature **531**, 206 (2016).
- ⁶⁵ A. Y. Kitaev, Annals of Physics **303**, 2 (2003).
- ⁶⁶ C. Nayak, S. H. Simon, A. Stern, M. Freedman, and S. Das Sarma, Rev. Mod. Phys. **80**, 1083 (2008).
- ⁶⁷ K. Flensberg, Phys. Rev. Lett. **106**, 090503 (2011).
- ⁶⁸ D. E. Liu and H. U. Baranger, Phys. Rev. B **84**, 201308 (2011).
- ⁶⁹ E. Vernek, P. H. Penteado, A. C. Seridonio, and J. C. Egues, Phys. Rev. B **89**, 165314 (2014).
- ⁷⁰ S. Hoffman, C. Schrade, J. Klinovaja, and D. Loss, Phys. Rev. B **94**, 045316 (2016).
- ⁷¹ M. T. Deng, S. Vaitiekenas, E. B. Hansen, J. Danon, M. Leijnse, K. Flensberg, J. Nygård, P. Krogstrup, and C. M. Marcus, Science **354**, 1557 (2016).
- ⁷² L. S. Ricco, Y. Marques, F. A. Dessotti, R. S. Machado, M. de Souza, and A. C. Seridonio, Phys. Rev. B **93**, 165116 (2016).
- ⁷³ F. A. Dessotti, L. S. Ricco, Y. Marques, L. H. Guessi, M. Yoshida, M. S. Figueira, M. de Souza, P. Sodano, and A. C. Seridonio, Phys. Rev. B **94**, 125426 (2016).
- ⁷⁴ L. A. Landau, S. Plugge, E. Sela, A. Altland, S. M. Albrecht, and R. Egger, Phys. Rev. Lett. **116**, 050501 (2016).
- ⁷⁵ C. Schrade, S. Hoffman, and D. Loss, Phys. Rev. B **95**, 195421 (2017).
- ⁷⁶ L. Xu, X.-Q. Li, and Q.-F. Sun, Journal of Physics: Condensed Matter **29**, 195301 (2017).
- ⁷⁷ E. Prada, R. Aguado, and P. San-Jose, Phys. Rev. B **96**, 085418 (2017).
- ⁷⁸ L. Fu and C. L. Kane, Phys. Rev. Lett. **102**, 216403 (2009).
- ⁷⁹ E. Prada, P. San-Jose, and R. Aguado, Phys. Rev. B **86**, 180503 (2012).
- ⁸⁰ J. S. Lim, R. López, and L. Serra, New Journal of Physics **14**, 083020 (2012).

- ⁸¹ A. A. Zyuzin, D. Rainis, J. Klinovaja, and D. Loss, *Phys. Rev. Lett.* **111**, 056802 (2013).
- ⁸² D. Rainis, L. Trifunovic, J. Klinovaja, and D. Loss, *Phys. Rev. B* **87**, 024515 (2013).
- ⁸³ A. Zazunov, A. Altland, and R. Egger, *New Journal of Physics* **16**, 015010 (2014).
- ⁸⁴ L. Weithofer, P. Recher, and T. L. Schmidt, *Phys. Rev. B* **90**, 205416 (2014).
- ⁸⁵ F. m. c. Crépin, B. Trauzettel, and F. Dolcini, *Phys. Rev. B* **89**, 205115 (2014).
- ⁸⁶ W. S. Cole, J. D. Sau, and S. Das Sarma, *Phys. Rev. B* **94**, 140505 (2016).
- ⁸⁷ P. Szumniak, D. Chevallier, D. Loss, and J. Klinovaja, *Phys. Rev. B* **96**, 041401 (2017).
- ⁸⁸ D. Sticlet, C. Bena, and P. Simon, *Phys. Rev. Lett.* **108**, 096802 (2012).
- ⁸⁹ M. Guigou, N. Sedlmayr, J. M. Aguiar-Hualde, and C. Bena, *EPL* **115**, 47005 (2016).
- ⁹⁰ D. Stanescu and S. Tewari, *Journal of the Indian Institute of Science* **96**, 107 (2016).
- ⁹¹ C.-X. Liu, J. D. Sau, T. D. Stanescu, and S. Das Sarma, *Phys. Rev. B* **96**, 075161 (2017).
- ⁹² C. Moore, T. D. Stanescu, and S. Tewari, *arXiv:1711.06256*.
- ⁹³ Y.-H. Chan, C.-K. Chiu, and K. Sun, *Phys. Rev. B* **92**, 104514 (2015).
- ⁹⁴ T. Gulden, M. Janas, Y. Wang, and A. Kamenev, *Phys. Rev. Lett.* **116**, 026402 (2016).
- ⁹⁵ J.-H. Park, G. Yang, J. Klinovaja, P. Stano, and D. Loss, *Phys. Rev. B* **94**, 075416 (2016).
- ⁹⁶ S. Tewari, J. D. Sau, V. W. Scarola, C. Zhang, and S. Das Sarma, *Phys. Rev. B* **85**, 155302 (2012).
- ⁹⁷ J. Klinovaja and D. Loss, *Phys. Rev. B* **86**, 085408 (2012).
- ⁹⁸ W. Wernsdorfer, *Superconductor Science and Technology* **22**, 064013 (2009).
- ⁹⁹ P. Stano, J. Klinovaja, A. Yacoby, and D. Loss, *Phys. Rev. B* **88**, 045441 (2013).
- ¹⁰⁰ T. Staudacher, F. Shi, S. Pezzagna, J. Meijer, J. Du, C. A. Meriles, F. Reinhard, and J. Wrachtrup, *Science* **339**, 561 (2013).
- ¹⁰¹ L. Trifunovic, F. L. Pedrocchi, S. Hoffman, P. Maletinsky, A. Yacoby, and D. Loss, *Nature Nanotechnology* **10**, 541 (2015).
- ¹⁰² M. J. Martínez-Pérez, B. Müller, D. Schwebius, D. Korinski, R. Kleiner, J. Sesé, and D. Koelle, *Superconductor Science and Technology* **30**, 024003 (2017).
- ¹⁰³ L. Thiel, D. Rohner, M. Ganzhorn, P. Appel, E. Neu, B. Müller, R. Kleiner, D. Koelle, and P. Maletinsky, *Nature Nanotechnology* **11**, 677 (2016).